frontiers in Earth Science

PERSPECTIVE
published: 28 September 2016
doi: 10.3389/feart.2016.00088

Inferring the Effects of Compositional Boundary Layers on Crystal Nucleation, Growth Textures, and Mineral Chemistry in Natural Volcanic Tephras through Submicron-Resolution Imaging

Georg F. Zellmer[1], Naoya Sakamoto[2], Shyh-Lung Hwang[3], Nozomi Matsuda[2], Yoshiyuki Iizuka[4], Anja Moebis[1] and Hisayoshi Yurimoto[2]*

[1] *Volcanic Risk Solutions, Institute of Agriculture and Environment, Massey University, Palmerston North, New Zealand,* [2] *Isotope Imaging Laboratory, Department of Natural History Sciences, Hokkaido University, Sapporo, Japan,* [3] *Department of Materials Science and Engineering, National Dong Hwa University, Hualien, Taiwan,* [4] *Institute of Earth Sciences, Academia Sinica, Taipei, Taiwan*

OPEN ACCESS

Edited by:
Oliver Jagoutz, Massachusetts Institute of Technology, USA

Reviewed by:
Christy B. Till, Arizona State University, USA
Fabio Arzilli, University of Manchester, UK

****Correspondence:***
Georg F. Zellmer
g.f.zellmer@massey.ac.nz

Specialty section:
This article was submitted to Petrology, a section of the journal Frontiers in Earth Science

Received: *28 July 2016*
Accepted: *15 September 2016*
Published: *28 September 2016*

Citation:
Zellmer GF, Sakamoto N, Hwang S-L, Matsuda N, Iizuka Y, Moebis A and Yurimoto H (2016) Inferring the Effects of Compositional Boundary Layers on Crystal Nucleation, Growth Textures, and Mineral Chemistry in Natural Volcanic Tephras through Submicron-Resolution Imaging. Front. Earth Sci. 4:88. doi: 10.3389/feart.2016.00088

Crystal nucleation and growth are first order processes captured in volcanic rocks and record important information about the rates of magmatic processes and chemical evolution of magmas during their ascent and eruption. We have studied glass-rich andesitic tephras from the Central Plateau of the Southern Taupo Volcanic Zone by electron- and ion-microbeam imaging techniques to investigate down to sub-micrometer scale the potential effects of compositional boundary layers (CBLs) of melt around crystals on the nucleation and growth of mineral phases and the chemistry of crystal growth zones. We find that CBLs may influence the types of mineral phases nucleating and growing, and growth textures such as the development of swallowtails. The chemistry of the CBLs also has the capacity to trigger intermittent overgrowths of nanometer-scale bands of different phases in rapidly growing crystals, resulting in what we refer to as cryptic phase zoning. The existence of cryptic phase zoning has implications for the interpretation of microprobe compositional data, and the resulting inferences made on the conditions of magmatic evolution. Identification of cryptic phase zoning may improve thermobarometric estimates and thus geospeedometric constraints. In future, a more quantitative characterization of CBL formation and its effects on crystal nucleation and growth may contribute to a better understanding of melt rheology and magma ascent processes at the onset of explosive volcanic eruptions, and will likely be of benefit to hazard mitigation efforts.

Keywords: crystal nucleation, crystal growth, swallow tail textures, cryptic phase zoning, Ngauruhoe volcano, Ruapehu volcano

INTRODUCTION

Crystal nucleation and growth are first-order processes in the evolution of silicate melts during cooling or degassing (e.g., Cashman and Marsh, 1988; Marsh, 1988; Fokin et al., 2006; Toramaru et al., 2008; Hammer, 2009; Hammer et al., 2010; Melnik et al., 2011) and determine mineral and melt chemistry and their evolution, which form the foundation of thermobarometric and hygrometric constraints (e.g., Putirka, 2008; Lange et al., 2009; Waters and Lange, 2015). Minerals may also provide critical insights into the rates of magmatic processes occurring during magma evolution and ascent at the onset of volcanic eruptions, with analytical methods ranging from crystal size distribution studies (e.g., Cashman and Marsh, 1988; Marsh, 1988, 1998; Hammer et al., 1999; Piochi et al., 2005; Noguchi et al., 2006, 2008; Clarke et al., 2007; Toramaru et al., 2008; Melnik et al., 2011) to diffusion geospeedometry (e.g., Zellmer et al., 1999, 2003, 2011, 2016; Morgan et al., 2004; Costa and Dungan, 2005; Martin et al., 2008; Druitt et al., 2012; Ruprecht and Plank, 2013). Thus, understanding the processes that govern crystal nucleation and growth, as well as crystal morphology, structure, and composition, are key to unlocking volcanic hazards and many other compelling questions. Small scale variations in crystal chemistry have become apparent in the last few decades through advances in microanalytical techniques (Anderson, 1983; Wallace and Bergantz, 2002; Davidson et al., 2007; Jerram and Martin, 2008, and references therein). At present, the most advanced instruments provide submicroscopic resolution (down to nanometer scale) of crystal chemistry and crystal structure (Zellmer et al., 2015, 2016). With increasing magnification, the small-scale complexity of compositional and structural variations has become apparent, elucidating magmatic processes that were previously not resolvable. In natural tephras, the latest small-scale variations are likely acquired at the onset or during eruption of the samples, and understanding such variations may thus be crucial in the characterization and mitigation of volcanic hazards (Zellmer et al., 2016).

In this perspective article, we focus on the narrow compositional boundary layers (CBLs) of melt around growing crystals (Zhang, 2009) and their potential effects on crystal nucleation, growth, and compositional as well as phase zoning, using as examples some tephras from New Zealand's recent Central Plateau eruptions in the Southern Taupo Volcanic Zone (Moebis, 2010; Moebis et al., 2011). CBLs are the interface-melt layers around growing or dissolving crystals with composition different to that of the bulk melt. CBLs develop when crystal growth or dissolution rates exceed the rate of diffusion of the crystal-forming ions within the melt. Their thicknesses therefore depend on growth/dissolution rate of the crystal, diffusion rate of the ions, and on the relative motion of crystal and melt (Levich, 1962). We demonstrate here through semiquantitative imaging techniques that there are complex interdependencies between CBLs and crystal nucleation, growth, and zoning. A detailed quantification of these interdependencies is beyond the scope of this contribution, but we argue that their study is important and may ultimately improve volcanic hazard characterization and mitigation strategies.

METHODS

Sampling Details and Sample Preparation

Tephra samples from the Central Plateau were collected by one of us (AM) for tephrochronological work. In the present study, we report data from Mangatawai tephra 407-28 and Papakai tephra 606-30 sourced from Ngauruhoe volcano, with ages of *c.* 2800 and *c.* 3980 cal. years B.P., respectively (Moebis, 2010), and from Tufa Trig tephra 108-137 (TF13 of Donoghue et al., 1997) sourced from Ruapehu volcano, with an age of *c.* 540 cal. years B.P. Volcanic glass shards from individual tephra units were handpicked at Massey University. The particles were embedded in an epoxy plug (EPOTEK 301), then cut and polished with diamond pastes of successively finer grades. The final polish was made at the Institute of Earth Sciences (IES), Academia Sinica, using a vibration polisher (Buhler: Vibromet-2) with 0.3 μm alumina compounds for several hours. For electron microbeam work, the polished specimens were then coated by a layer of carbon (Q150TE, Quorum Technologies Ltd., UK). For subsequent analysis by secondary ion mass spectrometry (SIMS), the carbon coat was removed with ethanol, and samples were coated with a thin film (*c.* 70 nm) of gold (SC-701MC, Sanyu Electron Co., Ltd.) at the Isotope Imaging Laboratory (IIL) of Hokkaido University.

Electron Probe Microanalysis

Crystals within tephra shards were analyzed at IES using a JEOL JXA-8900R electron microprobe equipped with four wavelength-dispersive spectrometers. A 2 μm defocused beam was operated for analysis at an acceleration voltage of 15 kV with a beam current of 12 nA. Measured X-ray intensities were ZAF-corrected using the standard calibration of synthetic (s) and natural (n) chemical-known standard minerals with various diffracting crystals, as follows: diopside (s) or wollastonite (s) for Si with TAP crystal, rutile (s) for Ti with PET crystal, corundum (s) for Al (TAP), chromium oxide (s) for Cr (PET), fayalite (s), or hematite (n) for Fe with LiF crystal, tephroite (s) for Mn (PET), periclase (s) for Mg (TAP), wollastonite (s) for Ca (PET), albite (n) for Na (TAP), and adularia (n) for K (PET). Peak and both upper and lower baseline X-rays were counted for 10 s for each element, respectively. Standards run as unknowns yielded major oxide relative standard deviations for Si, Na, and K of less than 1%, and less than 0.5% for other elements. Detection limits, based on 3σ of standard calibration, were less than 600 ppm for all elements.

Electron Microscopy and Isotopography

Backscattered electron (BSE) images were obtained using a field emission scanning electron microscope (FE-SEM; JEOL JSM-7000F) at the Isotope Imaging Laboratory (IIL), Hokkaido University, equipped with a high sensitivity energy dispersive X-ray spectrometer (EDS; Oxford X-Max 150). However, high-magnification work on crystal rims could not be conducted with this technique due to edge effects. Therefore, the IIL isotope microscope system, a Cameca ims-1270 SIMS instrument equipped with a stacked CMOS-type active pixel sensor (SCAPS) for ion imaging, was applied to visualize at high magnification the elemental distribution on the sample surface ("isotopography,"

for details see Yurimoto et al., 2003). An O- primary beam of 23 keV was irradiated on the sample surface of approximately 60 × 60 μm^2 with beam currents ranging from *c.* 1.5 to 20 nA. The exit slit was narrowed enough to eliminate the contribution of interference ions to the isotopic images. The positive secondary ion images of ^{23}Na, ^{24}Mg, ^{27}Al, ^{28}Si, ^{40}Ca, and ^{56}Fe on the sample surface were collected in a SCAPS detector, with exposure times ranging between 200 and 750 s. A spatial resolution of about 300 nm was achieved for our samples. Ablation rates of only about 1 μm/h allowed the successful acquisition of images at 5 s per frame of essentially the identical sample surface across all elements. Secondary ion intensity varied with primary beam intensity. Image gray scales were adjusted to balance these variations.

Transmission Electron Microscopy (TEM)

For TEM analyses, several samples of *c.* 50 nm thickness were prepared from the corona pyroxene overgrowing an olivine crystal of a selected Ruapehu tephra by applying the focused ion beam technique (FIB; SMI-3050). Selective area electron diffraction patterns and images were obtained using a transmission electron microscope (JEOL JEM-3010) operated at 300 kV. The instrument was equipped with an energy dispersive X-ray (EDX) spectrometer (Oxford EDS-6636) featuring an ultrathin window and a Si(Li) detector, capable of detection of elements from boron to uranium. EDX spectra were collected for 200 s. Semi-quantitative analysis was based on the Cliff-Lorimer thin film approximation with experimental k-factors obtained from natural minerals (Loretto, 1994).

RESULTS

Electron probe mineral chemical data are given in **Supplementary Table 1**. In summary, besides minor oxide phases that have not been analyzed but are present in all studied samples, Mangatawai tephra 407-28 contains crystals of plagioclase (An_{57-85}) and orthopyroxene ($En_{63-72}Fs_{23-27}Wo_{3-5}$); Papakai tephra 606-30 contains crystals of plagioclase (An_{45-85}) and orthopyroxene ($En_{67-73}Fs_{24-29}Wo_{3-5}$); and Tufa Trig tephra 108-137 contains crystals of plagioclase (An_{51-66}), orthopyroxene ($En_{63-84}Fs_{12-33}Wo_{3-5}$), clinopyroxene ($En_{44-55}Fs_{10-17}Wo_{35-43}$), and olivine ($Fo_{71-75}$).

The present study focusses on results from semi-quantitative high-resolution imaging. **Figures 1A–C** show SCAPS elemental maps of a large zoned plagioclase crystal, set in a glassy groundmass with microlites of plagioclase and pyroxene. A complexly zoned large plagioclase crystal experiencing synneusis (Vance, 1969; Dowty, 1980) with a microphenocryst (bottom right) is seen, with zoning particularly evident in the Na-image. Microlites show swallow-tail textures indicating rapid crystal growth. There is striking evidence of distinct CBLs of melt present around all crystals, about 1 micron in width. CBLs are enriched in Mg and depleted in Al and Na around plagioclase crystals, and vice versa around pyroxene microlites (cf. small pyroxene microlite in center right of image). Complex zoning of Na in plagioclase is evident even in the microlites, with a wavelength of similar width to the CBL. The black arrow in c indicates plagioclase nanolites forming just outside the CBL of the large plagioclase crystal, the white arrow points to a magnesian nanolite forming in the CBL. **Figure 1D** is a BSE image of groundmass microlites and nanolites of another sample. Pyroxene microlites have a Fe-rich rim and are surrounded by Fe-poor CBLs, similar in grayscale as plagioclase microlites. Magnetite nanolites are seen distributed throughout the groundmass, but the largest are surrounding the plagioclase microlites.

Figure 2 provides an analysis of an olivine crystal with pyroxene corona texture. Panel (a) shows the BSE image of part of this crystal set in a glassy groundmass. SCAPS elemental maps of the corona texture are provided for Mg (panel b) and Ca (panel c). Variations in Ca concentration within the overgrowth are evident, as observed previously in other corona orthopyroxenes (Zellmer et al., 2016), with a very strong enrichment in the rim of the overgrowth, and concomitant depletion in the CBL. Weaker Ca-enrichment zones are evident within the overgrowth. Such calcic lamellae are ubiquitous in overgrowth orthopyroxenes from the southern Taupo Volcanic Zone, and also occur in some orthopyroxene microphenocrysts (cf. Zellmer et al., 2016). Panels (d) and (e) are TEM bright field images of FIB sections, the location of which are indicated in panel (b). The images show clear phase boundaries of nm-thin layers of Ca-rich clinopyroxenes within Ca-poor orthopyroxene overgrowth. Two clinopyroxene domains can be identified by semiquantitative EDX spectrometry: domain A adjacent to the glass, with Al-enrichment (panel f), and domain B, inside the overgrowth, low in Al. Neither domain is in Fe/Mg exchange equilibrium with their orthopyroxene host, the EDX spectrum of which is provided in **Supplementary Image 1**. In equilibrium, K_D(Fe-Mg) should be 1.09 ± 0.14 (Putirka, 2008). Domain A yields a K_D(Fe-Mg) of >2.00, while domain B yields a K_D(Fe-Mg) of <0.80. Two-pyroxene thermobarometry therefore cannot be conducted.

DISCUSSION

Crystal nucleation may initially be randomly distributed within the glass, i.e., may be homogeneous (Fokin et al., 2006). However, crystal growth and associated CBL development appears to result in a more favorable nucleation environment of magnesian phases (such as pyroxene) in magnesian CBLs, which are less favorable for nucleation of Mg-poor phases (such as plagioclase) that will nucleate away from these CBLs (**Figure 1C**). Mg-poor phases will preferentially nucleate in Mg-poor CBLs. For example, preferential plagioclase nucleation would be expected in the CBLs developing around growing orthopyroxene crystals (further discussed below, cf. **Figure 1D**). Inhomogeneous crystal nucleation has previously been described (e.g., Hammer et al., 2010), and has recently been associated with CBLs that developed during dissolution of natural olivine in SiO_2-rich melts (Zellmer et al., 2016).

CBLs will be less depleted in crystal-forming elements at crystal corners, and this may be the reason for the development of swallow-tail textures (Vernon, 2004), which form by more

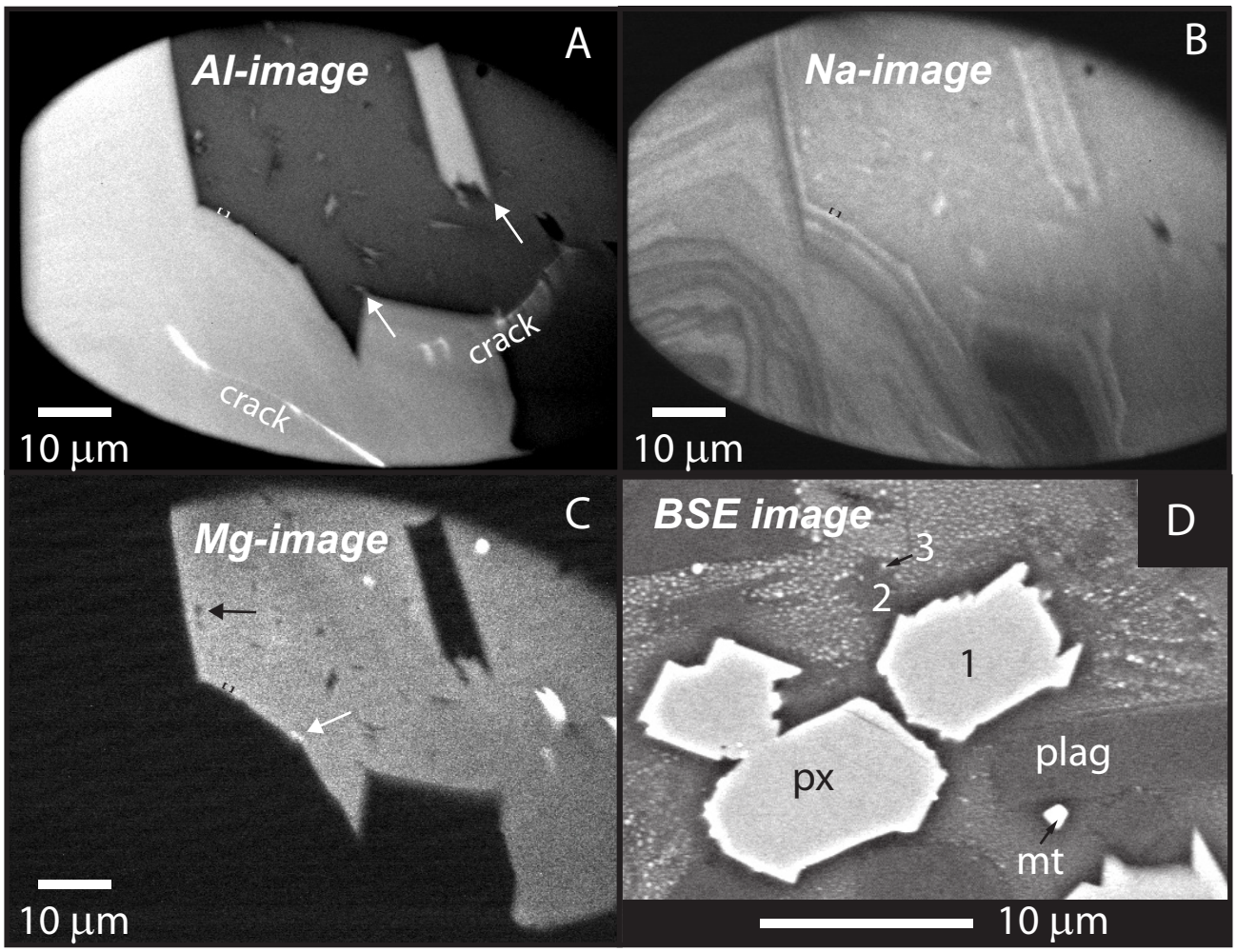

FIGURE 1 | (A–C) SCAPS elemental images of part of a complexly zoned plagioclase phenocryst in a glass shard with plagioclase and pyroxene microlites from Mangatawai tephra 407-28. Melt boundary layers around plagioclase, with their width indicated at one point in the image by square brackets, are depleted in Al and Na and enriched in Mg. Several microlites show swallowtail textures (cf. arrows in **A**). Two small cracks indicated in **(A)** result in localized imaging artifacts. Plagioclase and pyroxene nanolites discussed in the text are indicated by black and white arrows, respectively, in **(C)**. **(D)** SEM-image of swallow-tail textured pyroxene and plagioclase microlites, as well as magnetite nanolites, in a glass shard from Papakai tephra 606-30. Melt boundary layers around pyroxenes (px) are depleted in Fe. Plagioclase (plag) microlites nucleate in these boundary layers and grow outwards. Magnetite (mt) nanolites are preferentially found within melt boundary layers around plagioclase. Numbers indicate possible nucleation and growth sequence.

rapid crystal growth out from those corners in response to greater availability of crystal-forming elements within these local environments (**Figures 1A–C**). Crystal chemical zonation at circa 1 micron wavelength (**Figure 1B**) may be the response of CBL development at the same length scale, and subsequent CBL destruction, e.g., by movement of the crystal through the melt and concomitant erosion of the CBL, resulting in a regular local variations of ions available to the growing crystals. Such variations are even seen in microlites. Repetitive CBL development and destruction may thus represent an alternative way to form the fine-scale outer zoning in crystal composition observed in many volcanic phenocrysts, as opposed to being due to growth during magmatic rejuvenation and convection in subvolcanic reservoirs (cf. Shelley, 1993). Timescales predicted by modeling diffusion at intracrystalline boundaries of incompatible element enriched zones may thus not always be associated with magmatic intrusion events, for example, but instead might be recording timescales of crystallization during cooling or decompression-induced degassing.

As a result of these complex interactions of crystal nucleation and CBL formation by crystal growth, small scale heterogeneities in the mineral distribution of the groundmass may result. **Figure 1D** provides an example where orthopyroxene microlite growth has apparently resulted in Ca and Al enrichment of developing CBLs, which served as nucleation environments for plagioclase microlites. These, in turn, generated Fe-rich CBLs that represented favorable environments for nucleation of growth of magnetite nanolites.

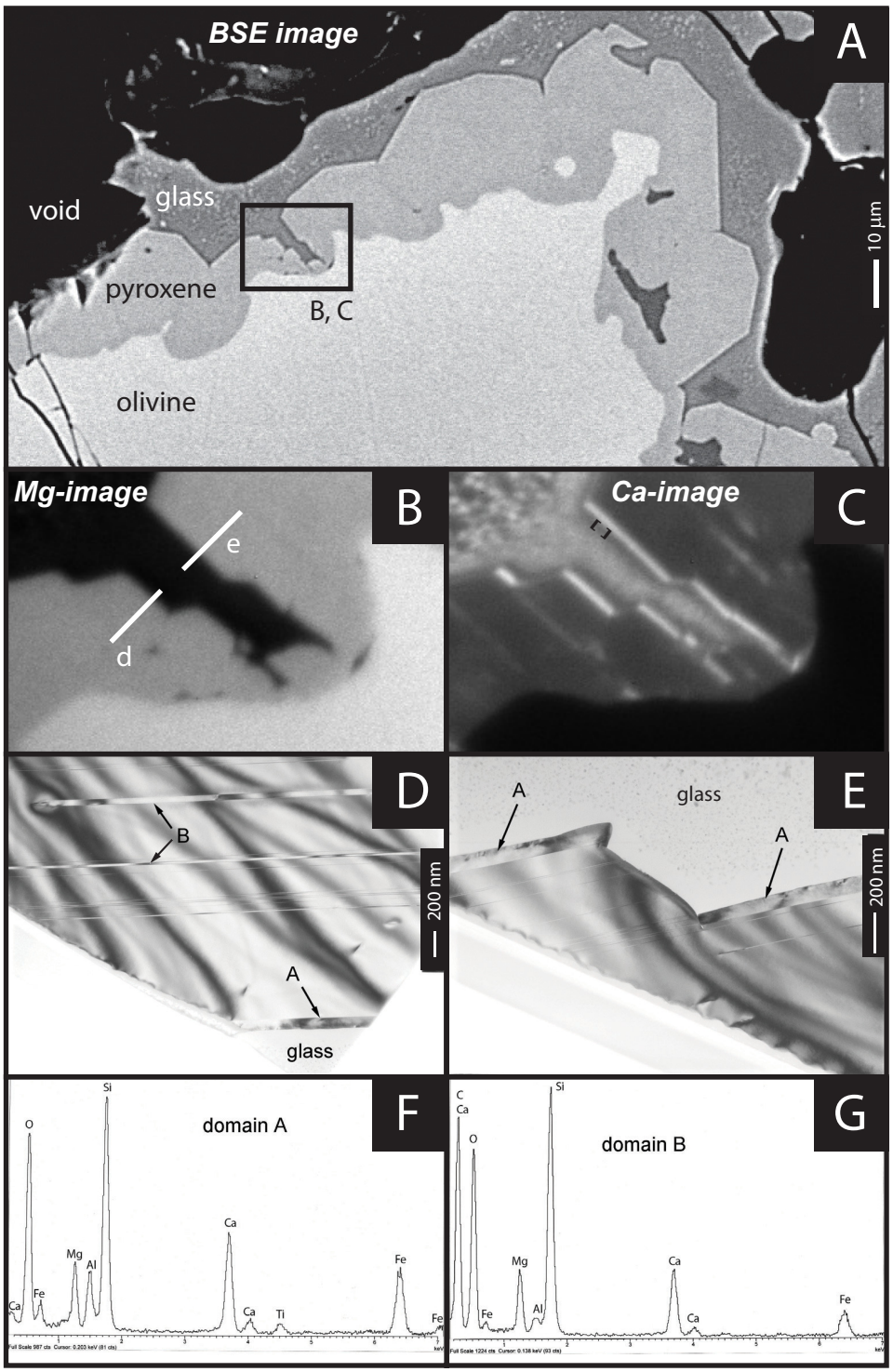

FIGURE 2 | Pyroxene corona textures on olivine displaying cryptic phase zoning in a glass shard from Tufa Trig tephra 108-137. (A) Backscattered electron image of part of the grain, indicating the area investigated by SCAPS imaging. **(B)** SCAPS Mg-image, showing the Mg-rich olivine (bright), the pyroxenes (gray), and the Mg-poor glass (dark). Position of focussed ion beam (FIB) sections for TEM work is indicated. **(C)** SCAPS Ca-image showing the Ca-poor olivine (dark), the dark-gray low-Ca pyroxene with some bright high-Ca bands, and the glass with variable Ca-content: low in the boundary layer (indicated by square brackets) right next to the outermost high-Ca growth zone, high in between the two pyroxene crystals, and highly variable away from the crystals. **(D,E)** TEM bright field images of FIB sections showing nm-scale bands of the high Ca-phase at the pyroxene rims (domain A), as well as inside the pyroxene crystal (domain B). Semi-quantitative analytical electron microscopy energy-dispersive X-ray spectra of high-Ca domains A and B are provided in **(F,G)**, respectively, yielding a higher-Ca, low Mg/Fe aluminous pyroxene in domain A and a lower-Ca, high Mg/Fe pyroxene in domain B. See **Supplementary Image 1** for the EDX spectrum of the orthopyroxene host crystal, provided for comparison.

The effect of CBLs may not only be restricted to variations in major (and presumably trace) element zonation in phases displaying solid solution, but may extend to triggering phase changes on microscopic to submicroscopic scales: **Figure 2** illustrates the submicroscopic phase changes within rapidly growing pyroxene crystals, which is what one may refer to as cryptic phase zoning. These lamellae are suggestive of exsolution textures, with clinopyroxene exsolving from orthopyroxene (e.g., Vernon, 2004). However, if this was the case, one would expect Fe/Mg exchange equilibrium between the host and exsolution zones. Although the EDX chemical analysis is only semiquantitative, given the narrow width of the clinopyroxene bands, the magnitude of the measured disequilibria of both clinopyroxene domains with their orthopyroxene host is likely too great to be attributable to analytical uncertainties. Thus, we prefer a scenario where rapid orthopyroxene growth results in a calcic CBL, which intermittently triggers brief precipitation intervals of clinopyroxene (domain B) instead of orthopyroxene. These intermittent intervals of clinopyroxene precipitation would then rapidly deplete the CBL in Ca, such that the system switches back to orthopyroxene as the preferred phase. Finally, domain A at the edge of the crystal likely represents growth related to quenching. In this scenario, cryptic phase zoning is related to crystal growth and associated chemical variations of the evolving CBL over time.

The presence of cryptic phase zoning in pyroxenes represents a challenge for two-pyroxene thermobarometry as well as pyroxene-melt thermobarometry (e.g., Putirka, 2008). Electron microprobe analysis (EMPA) is unable to resolve such submicron features and will yield average compositions with somewhat elevated amounts of calcium. Detailed imaging of submicron phase zonation may in future allow more successful targeting of crystal growth zones (cf. Zellmer et al., 2015) and thus may improve thermobarometric constraints. Temperature uncertainties still represent one of the principle limiting factors in diffusion geospeedometry (Costa and Morgan, 2010; Petrone et al., 2016), and tighter temperature constraints would be a significant advance in this respect.

Nucleation and growth of microlites are processes occurring during the last stage of magma ascent at the onset and during eruption of volcanic tephras (Hammer et al., 1999; Piochi et al., 2005; Noguchi et al., 2006, 2008; Clarke et al., 2007). Understanding these processes down to submicrometer scale is important to better characterize the crystallization of microlites in volcanic conduits, which have been used to estimate the timescales of magma ascent in order to characterize and mitigate the hazards of explosive volcanic eruptions (Zellmer et al., 2016). Our study shows that CBLs in natural magmas may significantly influence crystal nucleation and crystal growth, as well as the resulting crystal morphologies, crystal chemical zonation, and the distribution of small scale heterogeneities within the crystallizing groundmass. We have outlined some of the complex interplays of crystal nucleation, growth, CBL formation, and crystal chemical as well as phase zonation. Additional work will be required to properly quantify these processes, including the characterization of potential variations in the width of CBLs between different samples, and what this might reveal in terms of relative movement of crystals and melt, and thus about potential variations in melt rheology and melt ascent processes. Given the growing importance of the role of igneous petrology in informing volcanic hazards and their mitigation (Saunders et al., 2012), we anticipate significant advances in this field in the near future.

AUTHOR CONTRIBUTIONS

GFZ designed the project, assisted with analytical work, interpreted the data and wrote the paper. SH undertook TEM analyses. NS and NM undertook SEM and SIMS imaging work. YI undertook EPMA work. NS and HY checked SEM and SIMS data quality. AM collected and prepared the samples. All authors contributed to the discussion of results.

ACKNOWLEDGMENTS

We thank Fred Davis and Bob Stewart for useful discussions and Oliver Jagoutz for editorial handling of this contribution. We are grateful for constructive comments of Fabio Arzilli and Christy B. Till, which improved the script. GFZ acknowledges funding through the Ministry of Business, Innovation and Employment (MBIE, grant MAUX1507), and the National Geographic Society (grant 9577-14).

SUPPLEMENTARY MATERIAL

The Supplementary Material for this article can be found online at: http://journal.frontiersin.org/article/10.3389/feart.2016.00088

Supplementary Table 1 | Electron microprobe data of plagioclase, orthopyroxene, clinopyroxene, and olivine crystals from the studied tephras.

Supplementary Image 1 | EDX spectrum of the orthopyroxene host of the cryptic phase zonation (see text for details).

REFERENCES

Anderson, A. T. Jr. (1983). Oscillatory zoning of plagioclase: Nomarski interference contrast microscopy of etched polished sections. *Am. Mineral.* 68, 125–129.

Cashman, K. V., and Marsh, B. D. (1988). Crystal size distribution (CSD) in rocks and the kinetics and dynamics of crystallisation. II: Makaopuhi lava lake. *Contrib. Mineral. Petrol.* 99, 292–305. doi: 10.1007/BF00375363

Clarke, A. B., Stephens, S., Teasdale, R., Sparks, R. S. J., and Diller, K. (2007). Petrologic constraints on the decompression history of magma prior to Vulcanian explosions at the Soufrière Hills volcano, Montserrat. *J. Volcanol. Geother. Res.* 161, 261–274. doi: 10.1016/j.jvolgeores.2006.11.007

Costa, F., and Dungan, M. (2005). Short time scales of magmatic assimilation from diffusion modeling of multiple elements in olivine. *Geology* 33, 837–840. doi: 10.1130/G21675.1

Costa, F., and Morgan, D. J. (2010). "Time constraints from Chemical Equilibration in Magmatic Crystals," in *Timescales of Magmatic Processes: From Core to Atmosphere*, eds A. Dosseto, S. P. Turner, and J. A. Van Orman (Chichester: John Wiley & Sons, Ltd.), 125–159.

Davidson, J. P., Morgan, D. J., and Charlier, B. L. A. (2007). Frontiers in textural and microgeochemical analysis: isotopic microsampling of magmatic rocks. *Elements* 3, 253–259. doi: 10.2113/gselements.3.4.253

Donoghue, S. L., Neall, V. E., Palmer, A. S., and Stewart, R. B. (1997). The volcanic history of Ruapehu during the past 2 millennia based on the record of Tufa Trig tephras. *Bull. Volcanol.* 59, 136–146. doi: 10.1007/s004450050181

Dowty, E. (1980). Synneusis reconsidered. *Contrib. Mineral. Petrol.* 74, 75–84. doi: 10.1007/BF00375491

Druitt, T. H., Costa, F., Deloule, E., Dungan, M., and Scaillet, B. (2012). Decadal to monthly timescales of magma transfer and reservoir growth at a caldera volcano. *Nature* 482, 77–80. doi: 10.1038/nature10706

Fokin, V. M., Zanotto, E. D., Yuritsyn, N. S., and Schmelzer, J. W. P. (2006). Homogeneous crystal nucleation in silicate glasses: a 40 years perspective. *J. Non-Crystal. Solids* 352, 2681–2714. doi: 10.1016/j.jnoncrysol.2006.02.074

Hammer, J. E. (2009). Capturing crystal growth. *Geology* 37, 1055–1056. doi: 10.1130/focus112009.1

Hammer, J. E., Cashman, K. V., Hoblitt, R. P., and Newman, S. (1999). Degassing and microlite crystallization during pre-climactic events of the 1991 eruption of Mt. Pinatubo, Philippines. *Bull. Volcanol.* 60, 355–380. doi: 10.1007/s004450050238

Hammer, J. E., Sharp, T. G., and Wessel, P. (2010). Heterogeneous nucleation and epitaxial crystal growth of magmatic minerals. *Geology* 38, 367–370. doi: 10.1130/G30601.1

Jerram, D. A., and Martin, V. M. (2008). "Understanding crystal populations and their significance through the magma plumbing system," in *Dynamics of Crustal Magma Transfer, Storage and Differentiation,* eds C. Annen and G. F. Zellmer (London: Geological Society), 133–148.

Lange, R. A., Frey, H. M., and Hector, J. (2009). A thermodynamic model for the plagioclase-liquid hygrometer/thermometer. *Am. Mineral.* 94, 494–506. doi: 10.2138/am.2009.3011

Levich, V. G. (1962). *Physicochemical Hydrodynamics*. Englewood Cliffs, NJ: Prentic-Hall.

Loretto, H. M. (1994). *Electron Beam Analysis of Materials*. London: Chapman & Hall.

Marsh, B. D. (1988). Crystal size distribution (CSD) in rocks and the kinetics and dynamics of crystallisation. I: Theory. *Contrib. Mineral. Petrol.* 99, 277–291. doi: 10.1007/BF00375362

Marsh, B. D. (1998). On the interpretation of crystal size distributions in magmatic systems. *J. Petrol.* 39, 553–599. doi: 10.1093/petroj/39.4.553

Martin, V. M., Morgan, D. J., Jerram, D. A., Caddick, M. J., Prior, D. J., and Davidson, J. P. (2008). Bang! Month-scale eruption triggering at Santorini volcano. *Science* 321, 1178. doi: 10.1126/science.1159584

Melnik, O. E., Blundy, J. D., Rust, A. C., and Muir, D. D. (2011). Subvolcanic plumbing systems imaged through crystal size distributions. *Geology* 39, 403–406. doi: 10.1130/G31691.1

Moebis, A. (2010). *Understanding the Holocene Explosive Eruption Record of the Tongariro Volcanic Centre*. PhD thesis, Massey University, Palmerston North.

Moebis, A., Cronin, S. J., Neall, V. E., and Smith, I. E. (2011). Unravelling a complex volcanic history from fine-grained, intricate Holocene ash sequences at the Tongariro Volcanic Centre, New Zealand. *Q. Int.* 246, 352–363. doi: 10.1016/j.quaint.2011.05.035

Morgan, D. J., Blake, S., Rogers, N. W., De Vivo, B., Rolandi, G., Macdonald, R., et al. (2004). Time scales of crystal residence and magma chamber volume from modelling of diffusion profiles in phenocrysts: Vesuvius 1944. *Earth Planet. Sci. Lett.* 222, 933–946. doi: 10.1016/j.epsl.2004.03.030

Noguchi, S., Toramaru, A., and Nakada, S. (2008). Relation between microlite textures and discharge rate during the 1991-1995 eruptions at Unzen, Japan. *J. Volcanol. Geother. Res.* 175, 141–155. doi: 10.1016/j.jvolgeores.2008.03.025

Noguchi, S., Toramaru, A., and Shimano, T. (2006). Crystallization of microlites and degassing during magma ascent: constraints on the fluid mechanical behaviour of magma during the Tenjo Eruption on Kozu Island, Japan. *Bull. Volcanol.* 68, 432–449. doi: 10.1007/s00445-005-0019-4

Petrone, C. M., Braschi, B., and Tommasini (2016). Pre-eruptive magmatic processes re-timed using a non-isothermal approach to magma chamber dynamics. *Nat. Commun*. 7:12946. doi: 10.1038/ncomms12946

Piochi, M., Mastrolorenzo, G., and Pappalardo, L. (2005). Magma ascent and eruptive processes from textural and compositional features of Monte Nuovo pyroclastic products, Campi Flegrei, Italy. *Bull. Volcanol.* 67, 663–678. doi: 10.1007/s00445-005-0410-1

Putirka, K. D. (2008). "Thermometers and barometers for volcanic systems," in *Reviews in Mineralogy and Geochemistry,* Vol. 69, eds K. D. Putirka and F. Tepley (Chantilly, VA: Mineralogical Society of America), 61–120.

Ruprecht, P., and Plank, T. (2013). Feeding andesitic eruptions with a high-speed connection from the mantle. *Nature* 500, 68–72. doi: 10.1038/nature12342

Saunders, K., Blundy, J., Dohmen, R., and Cashman, K. (2012). Linking petrology and seismology at an active volcano. *Science* 336, 1023–1027. doi: 10.1126/science.1220066

Shelley, D. (1993). *Igneous and Metamorphic Rocks under the Microscope: Classification, Textures, Microstructures and Mineral Preferred Orientation.* London: Chapman & Hall.

Toramaru, A., Noguchi, S., Oyoshihara, S., and Tsune, A. (2008). MND (microlite number density) water exsolution rate meter. *J. Volcanol. Geother. Res.* 175, 156–167. doi: 10.1016/j.jvolgeores.2008.03.035

Vance, J. A. (1969). On synneusis. *Contrib. Mineral. Petrol.* 24, 7–29. doi: 10.1007/BF00398750

Vernon, R. H. (2004). *A Practical Guide to Rock Microstructure*. Cambridge, New York, NY; Madrid, Cape Town; Singapore, Sao Paulo, New Delhi: Cambridge University Press.

Wallace, G. S., and Bergantz, G. W. (2002). Wavelet-based correlation (WBC) of zoned crystal populations and magma mixing. *Earth Planet. Sci. Lett.* 202, 135–145. doi: 10.1016/S0012-821X(02)00762-8

Waters, L. E., and Lange, R. A. (2015). An updated calibration of the plagioclase-liquid hygrometer-thermometer applicable to basalts through rhyolites. *Am. Mineral.* 100, 2172–2184. doi: 10.2138/am-2015-5232

Yurimoto, H., Nagashima, K., and Kunihiro, T. (2003). High precision isotope micro-imaging of materials. *Appl. Surface Sci.* 203–204, 793. doi: 10.1016/S0169-4332(02)00825-5

Zellmer, G. F., Blake, S., Vance, D., Hawkesworth, C., and Turner, S. (1999). Plagioclase residence times at two island arc volcanoes (Kameni islands, Santorini, and Soufriere, St. Vincent) determined by Sr diffusion systematics. *Contrib. Mineral. Petrol.* 136, 345–357. doi: 10.1007/s004100050543

Zellmer, G. F., Hawkesworth, C. J., Sparks, R. S. J., Thomas, L. E., Harford, C., Brewer, T. S., et al. (2003). Geochemical evolution of the Soufrière Hills volcano, Montserrat, Lesser Antilles Volcanic Arc. *J. Petrol.* 44, 1349–1374. doi: 10.1093/petrology/44.8.1349

Zellmer, G. F., Hwang, S.-L., Sakamoto, N., Iizuka, Y., Harada, S., Kimura, J. -I., et al. (2015). "Interaction of arc magmas with subvolcanic hydrothermal systems: insights from compositions and metasomatic textures of olivine crystals in fresh basalts of Daisen and Mengameyama, Western Honshu, Japan," in *The Role of Volatiles in the Genesis, Evolution and Eruption of Arc Magmas,* eds G. F. Zellmer, M. Edmonds, and S. M. Straub (London: Geological Society; Special Publications), 219–236.

Zellmer, G. F., Rubin, K. H., Dulski, P., Iizuka, Y., Goldstein, S. L., and Perfit, M. R. (2011). Crystal growth during dike injection of MOR basaltic melts: evidence from preservation of local Sr disequilibria in plagioclase. *Contrib. Mineral. Petrol.* 161, 153–173. doi: 10.1007/s00410-010-0518-y

Zellmer, G. F., Sakamoto, N., Matsuda, N., Iizuka, Y., Moebis, A., and Yurimoto, H. (2016). On progress and rate of the peritectic reaction $Fo + SiO_2 \rightarrow En$ in natural andesitic arc magmas. *Geochim. Cosmochim. Acta* 185, 383–393. doi: 10.1016/j.gca.2016.01.005

Zhang, Y. (2009). *Geochemical Kinetics*. Princeton, NJ: Princeton University Press.

Conflict of Interest Statement: The authors declare that the research was conducted in the absence of any commercial or financial relationships that could be construed as a potential conflict of interest.